CHEMISTRY OF MATERIALS

ARTICLE

pubs.acs.org/cm

Structure and Transport Properties of Double-Doped $CoSb_{2.75}Ge_{0.25-x}Te_x$ ($x = 0.125-0.20$) with in Situ Nanostructure

Xianli Su,[†,‡] Han Li,[†] Guoyu Wang,[‡] Hang Chi,[‡] Xiaoyuan Zhou,[‡] Xinfeng Tang,[*,†] Qingjie Zhang,[†] and Ctirad Uher[*,‡]

[†]State Key Laboratory of Advanced Technology for Materials Synthesis and Processing, Wuhan University of Technology, Wuhan 43007, China

[‡]Department of Physics, University of Michigan, Ann Arbor, Michigan 48109, United States

ABSTRACT: Single-phase skutterudite compounds of composition $CoSb_{2.75}Ge_{0.25-x}Te_x$ ($x = 0.125-0.20$) were synthesized by the traditional melt-quench-anneal technique followed by spark plasma sintering. Rather than filling the skutterudite structure to reduce the thermal conductivity, the aim here is to use disorder on the pnicogen rings created by doping with both Te and Ge. Since heat-carrying phonons in $CoSb_3$ are those associated with the vibrational modes of the Sb-rings, such disorder should be effective in suppressing heat transport. The electrical transport properties can be tuned by adjusting the relative content of Te and Ge. The electrical conductivity and the thermoelectric power factor of the samples increase with the increasing Te content while the absolute value of the Seebeck coefficient decreases. Compared with the undoped $CoSb_3$, the lattice thermal conductivity is significantly suppressed because of an enhanced solubility of Te leading to an increase in the number of pnicogen rings being distorted. High resolution transmission electron microscopy images reveal an in situ nanostructure consisting of circular, 30 nm diameter dots of a skutterudite phase enriched with the dopants that are embedded in the skutterudite matrix poor in Ge and Te. Apart from phonon point-defect scattering, this nanostructure may also contribute to the overall low lattice thermal conductivity. The thermoelectric figure of merit for the $CoSb_{2.75}Ge_{0.05}Te_{0.20}$ compound reaches values in excess of 1.1 at 800 K. This value is competitive with single-filled n-type skutterudite compounds.

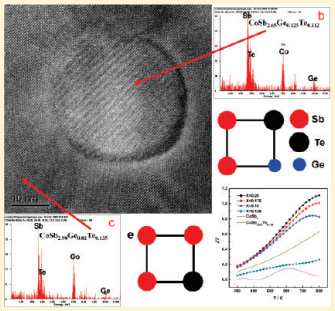

KEYWORDS: thermoelectric properties, in-situ nanostructure, skutterudite, point defect

INTRODUCTION

Thermoelectric (TE) materials are able to convert heat to electricity by purely solid state means. Thermoelectricity has attracted considerable attention as a viable process to convert waste industrial heat into usable electricity as well as for utilization of the solar thermal radiation for environmentally friendly power generation.[1−3] The efficiency of a TE material is closely related to the dimensionless figure of merit ZT, defined as $ZT = \alpha^2\sigma T/\kappa$, where α, σ, κ, and T are the Seebeck coefficient, electrical conductivity, total thermal conductivity, and absolute temperature, respectively. To achieve high efficiency, a large ZT is required.

Recently $CoSb_3$-based skutterudites have received considerable attention as prospective novel TE materials because of their unique crystal structure and excellent electronic transport properties.[2,4] Binary skutterudites are cubic compounds with the chemical formula MX_3 where M is a transition metal atom (Co, Rh, or Ir) and X is a pnicogen atom (P, As or Sb). They have small band gaps and possess high carrier mobilities, particularly in the case of p-type skutterudites.[5] Unfortunately, the thermal conductivity of binary skutterudites is also high, and this has been a serious impediment to their applications as TE materials. There are numerous ways how one can influence and lower the thermal conductivity of a structure. In the case of skutterudites, the most effective approach turned out to be filling of the structural voids by foreign elements[2,3,6] and this recipe has been explored and followed for the past dozen or so years with impressive improvements in the figure of merit of n-type filled skutterudites.[7,8] Recently, much attention has been paid to the possibility of importing benefits of lower-dimensional TE structures into the bulk matrix.[9] Specifically, incorporation of nanometer-scale inclusions in the bulk structure appears highly prospective for a dramatic lowering of the lattice thermal conductivity as the nanometer-scale structural features have a potential to strongly scatter heat-carrying phonons.[10−12] It is important to recognize that not just any nanostructure will do. The nanostructure of interest must preferably scatter phonons while leaving the carrier transport substantially unimpeded. Moreover, such a nanostructure must be stable at the temperature regime where the TE converter will operate. The limited experience suggests that nanostructures formed via processes such as spinodal decomposition,[10] matrix encapsulation,[13] nucleation and growth,[14] and special heat treatment processes[15] are inherently more stable than nanostructures brought into the matrix by external means. Moreover, the nanostructures of the first kind tend to be coherent with the matrix, and this assures minimal disturbance to the mean-free path of charge carriers.

Received: February 23, 2011
Revised: May 1, 2011
Published: May 19, 2011

Dominant heat-carrying phonons in skutterudites are associated with vibrations of pnicogen rings.[16,17] Therefore, changes in the phonon vibration spectra created by substitutions on the rings or by deforming the rings should decrease the lattice thermal conductivity. Often, tellurium has been tried as a dopant on the pnicogen rings.[18,19] However, its solubility is rather low, and the resulting change in the thermal conductivity upon doping is only modest. Recently, Liu et al.[20] prepared double-doped skutterudite compounds based on Sn and Te doping of $CoSb_3$ by mechanical alloying followed by spark plasma sintering. The presence of the group IV Sn compensates for the charge of the group VI Te and, in turn, increases its solubility to $x \sim 0.2$. The authors of ref 17 noted that their double-doped compounds have lower thermal conductivity than the single-doped skutterudites which they explained as a result of the combined influence of the grain boundary scattering and the point defect scattering. They also mentioned that on high resolution TEM images of their samples they detected "black regions" that they tentatively associated with nanodots of the kind seen in the LAST materials[10] and speculated that they might contribute to the overall low thermal conductivity. It is difficult to make a definitive statement regarding the influence of nanodots on the thermal transport in their samples since the authors provided no evidence for the chemical contrast between the matrix and the "black region" of their HRTEM images. Moreover, because their compounds had an average grain size of 140 nm, it is difficult to ascertain whether the reduction in the thermal conductivity is due to a small grain size on account of ball milling or the consequence of any possible nanostructure originating from a segregated nanophase.

To ascertain the presence of nanoinclusions upon double doping on the pnicogen rings and to find out their influence on transport properties, we synthesized a series of skutterudite compounds of composition $CoSb_{2.75}Ge_{0.25-x}Te_x$ with x = 0.125−0.20. In contrast to ref 20, our samples were prepared by the traditional method of synthesis based on quenching the melt and subjecting the ingots to a long-term annealing to achieve a pure skutterudite phase. The average grain size of our samples is on the scale of tens of micrometers, the length scale on which phonon scattering cannot be confused with the influence of nanometer-scale inclusions. We indeed detect such nanoiclusions in our HRTEM images, and we provide chemical contrast between them and the matrix.

EXPERIMENTAL SECTION

Skutterudite compounds were synthesized using high purity Sb(6N), Co(4N), Te(6N), and Ge(4N) starting materials. Stoichiometric amounts of constituents were weighed in a glovebox under high-purity Ar to prepare $CoSb_{2.75}Ge_{0.25-x}Te_x$ with x in the range from 0.125 to 0.20. The charge was sealed in a carbon-coated silica tube under the pressure of 10^{-3} Pa. The charge was melted and kept at 1373 K for 30 h. Subsequently, ampules with the melt were quenched in a supersaturated salt water bath, and ingots were annealed at 873 K for 7 days. The obtained material was ground in a glovebox into a fine powder and sintered by SPS at 923 K for 5 min under the pressure of 40 MPa.

The structure was characterized by X-ray diffraction (XRD, PANalytical X'Pert Pro X-ray diffraction using Cu $K\alpha$). The morphology and element content were determined by back scattered electron imaging (FESEM, S-4800) and energy dispersive X-ray (EDX) analysis (EDS, Horiba 250). The microstructure was investigated using transmission electron microscopy (TEM; JEM2100F) with energy-dispersive spectrometry (EDS). Hall effect measurements were performed from 5 K to 300 K in a cryostat equipped with a 5.5 T superconducting magnet. The high temperature Hall measurements were carried out in a home-built apparatus. Procedures for low temperature property measurements were the same as described elsewhere.[21] For measurements at high temperatures we relied on a ZEM-1 apparatus (electrical conductivity σ and the Seebeck coefficient α) and thermal conductivity κ was calculated from the measured thermal diffusivity D, specific heat C_p, and density d according to the relationship $\kappa = D \times C_p \times d$. The thermal diffusivity and the specific heat were determined using a laser flash method (NETZSCH: LFA 457) and a power-compensation differential scanning calorimeter (TA: DSCQ20), respectively. Uncertainties in the electrical conductivity, thermopower, and thermal conductivity measurements are ±5%, ± 5%, and ±7%, respectively.

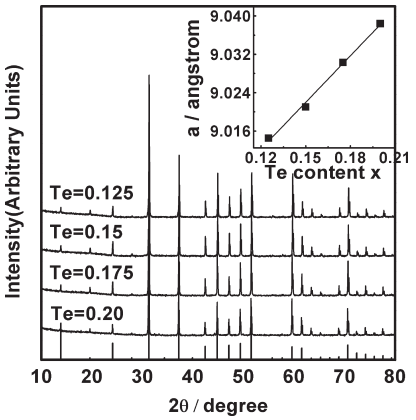

Figure 1. XRD patterns of $CoSb_{2.75}Ge_{0.25-x}Te_x$ (x = 0.125−0.20) samples.

RESULTS AND DISCUSSION

Composition and Structure of Specimens. Figure 1 shows the typical XRD patterns obtained on $CoSb_{2.75}Ge_{0.25-x}Te_x$ (x = 0.125−0.20) compounds with different Te doping contents x. The XRD patterns demonstrate that all bulk materials are single-phase skutterudite structures without any impurity phases such as GeTe and $CoTe_2$ according to JSPDS78-0976. Therefore, co-doping with Ge and Te in the above range of x does not change the crystal structure. The lattice constant increases in proportion to the relative amount of Te doped into the structure (see inset of Figure 1). This is understood based on the ionic radius of Te (97 pm) which is larger than that of Sb (76 pm) and consistent with the previous studies of Te doping in $CoSb_3$.[18−20] The linear increase of the lattice constant with x indicates that Te and Ge are being substituted on the Sb sites of the $CoSb_3$ crystal structure. For samples of $CoSb_{2.75}Ge_{0.05}Te_{0.20}$ and $CoSb_{2.75}Ge_{0.075}Te_{0.175}$, the solid solubility of Te on the Sb site exceeds the solubility of single-doped Te (x = 0.15)[18,19] because of partial charge compensation by Ge. The respective valence electron counts of Ge, Sb, and Te are 4, 5, and 6. A Ge atom substituting for Sb on the square 4-member Sb ring compensates for the charge of Te substituted for Sb on the same ring and effectively increases solid solubility of Te in $CoSb_3$. This is similar to the case of co-doped Te and Sn in $CoSb_3$.[20]

Figures 2a and 2b display the backscattered electron image (BSEI) and the secondary electron images for the polished surface of $CoSb_{2.75}Ge_{0.05}Te_{0.20}$, respectively. The results indicate a perfectly homogeneous chemical composition without the presence of any obvious secondary phase. To further study the

dx.doi.org/10.1021/cm200560s |Chem. Mater. 2011, 23, 2948–2955

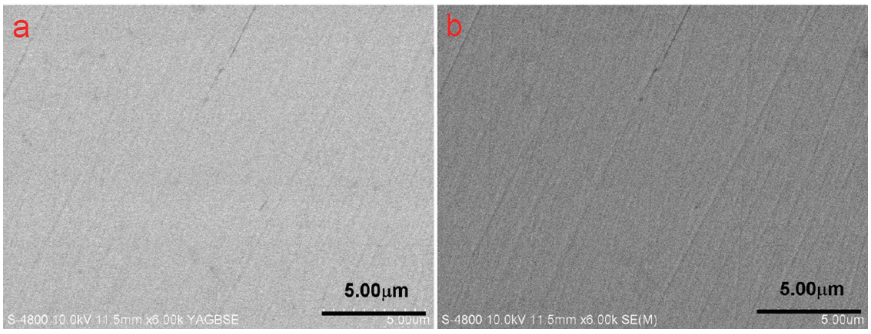

Figure 2. (a) Back scattered electron image. (b) Secondary electron images for $CoSb_{2.75}Ge_{0.05}Te_{0.20}$ sample.

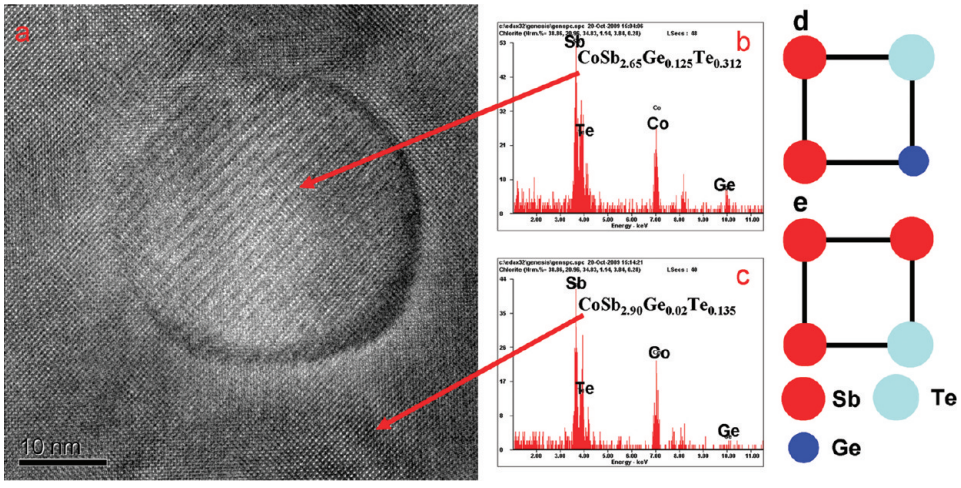

Figure 3. (a) TEM image of $CoSb_{2.75}Ge_{0.05}Te_{0.20}$. (b) EDS of the nanostructured region. (c) EDS of the matrix, (d) the pnicogen ring co-substituted by Ge and Te, and (e) the pnicogen ring substituted by Te.

microstructure, we used a transmission electron microscope (TEM). The data are shown in Figure 3a. We observe a nanostructure that exhibits a circular shape with the diameter of about 30 nm embedded in the matrix. The grain boundary is clearly visible separating the nanostructure and the matrix. Semiquantitative EDS results give the normalized chemical composition of the matrix (Figure 3c) and of the nanostructured phase (Figure 3b) as $CoSb_{2.90}Ge_{0.02}Te_{0.135}$ and $CoSb_{2.65}Ge_{0.125}Te_{0.312}$, respectively, which indicates that the nanostructured phase is rich in Ge and Te while the matrix is a region poor in Ge and Te. A completely homogeneous dispersion of Ge and Te in the skutterudite lattice would require a complete separation of Ge and Te atoms over long distances, which could create charge imbalances in the vicinity of these atoms. To achieve electroneutrality, it is more favorable for Ge to sit on the same pnicogen ring where Te is already located (Figure 3d). The presence of Ge thus not only tends to increase the solid solubility limit of Te, but it also leads to the in situ formation of a nanostructure. The formation mechanism of the nanostructure is akin to the case of the LAST and TAGS systems.[10,22,23]

Electrical Transport Properties of $CoSb_{2.75}Ge_{0.25-x}Te_x$ (x = 0.125−0.20). The temperature dependence of the electrical conductivity for $CoSb_{2.75}Ge_{0.25-x}Te_x$ (x = 0.125−0.20) compounds is shown in Figure 4. Except for the compensated sample $CoSb_{2.75}Ge_{0.125}Te_{0.125}$, all samples behave as highly degenerate semiconductors with their electrical conductivity decreasing as

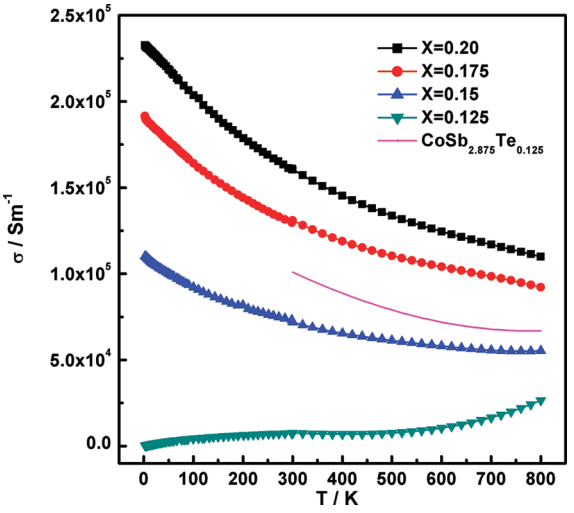

Figure 4. Electrical conductivity as a function of temperature for $CoSb_{2.75}Ge_{0.25-x}Te_x$.

the temperature increases. The compensated sample, in contrast, displays a typical nondegenerate semiconducting behavior. The doping effect of Te is clearly reflected in the enhanced value of the electrical conductivity that reaches 1.60×10^5 S/m at 300 K for $CoSb_{2.75}Ge_{0.05}Te_{0.20}$. Using equation $\sigma = \sigma_0 \exp(-E_g/2k_BT)$,

dx.doi.org/10.1021/cm200560s |Chem. Mater. 2011, 23, 2948–2955

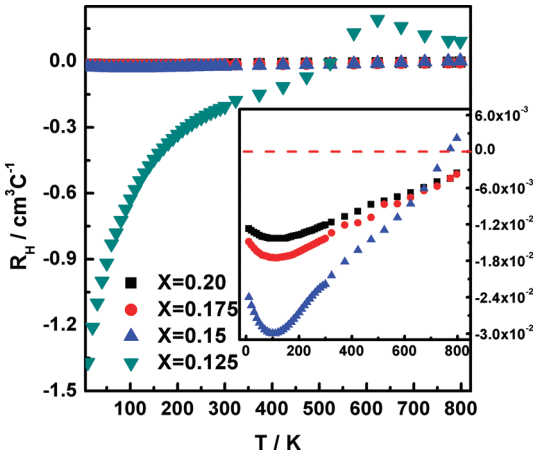

Figure 5. Hall coefficient as a function of temperature for $CoSb_{2.75}Ge_{0.25-x}Te_x$.

Table 1. Nominal Composition and Some Properties of $CoSb_{2.75}Ge_{0.25-x}Te_x$ Compounds at 300 K

nominal composition	σ (10^4 S/m)	R_H (cm^3/C)	N_p (10^{19}/cm^3)	μ_H (cm^2/(V s))
$CoSb_{2.75}Ge_{0.05}Te_{0.20}$	16.0	−0.0121	51.6	19.4
$CoSb_{2.75}Ge_{0.075}Te_{0.175}$	13.0	−0.0143	43.7	18.5
$CoSb_{2.75}$ $Ge_{0.10}Te_{0.15}$	7.3	−0.0219	28.6	16
$CoSb_{2.75}Ge_{0.125}Te_{0.125}$	0.75	−0.205	3.0	15.3

we attempted to fit the high temperature electrical conductivity of the compensated sample to obtain an estimate of the band gap E_g. The fit returned the value of E_g = 0.43 eV, consistent with the literature values.[24,25]

In Figure 5, we plot the Hall coefficient R_H as a function of temperature for $CoSb_{2.75}Ge_{0.25-x}Te_x$ (x = 0.125−0.20) compounds. All samples show negative R_H indicating that electrons are the dominant charge carrier. Samples with x = 0.15, 0.175, and 0.20 show a weak temperature dependence of R_H (in fact, on the scale of Figure 5 they are essentially temperature independent, and we need to expand the scale such as in the inset of Figure 5 to see the effect of temperature). In contrast, the compensated sample $CoSb_{2.75}Ge_{0.125}Te_{0.125}$ displays strong temperature dependence in R_H, and its absolute value decreases rapidly with the increasing temperature. At the highest temperatures of the experiment, a positive Hall coefficient is observed. Undoubtedly, this is the consequence of an early onset of intrinsic conduction with a strong participation of mobile holes. A much weaker temperature dependence of the uncompensated samples (x = 0.15, 0.175, and 0.20) in the inset of Figure 5 is similar to the temperature dependence of the Hall effect observed in lightly Ni-doped $CoSb_3$.[25] In particular, the minima on the curves near 100 K (deeper and more pronounced at smaller Te concentrations) are a footprint of the crossover from the predominantly impurity conduction to band conduction.[24,25] Assuming that at 300 K the transport is dominated by single band conduction, the room temperature values of the electron density are listed in Table 1.

Room temperature carrier mobility (μ_H) as a function of the carrier concentration (n) is shown in Figure 6. For comparison, we also display the data for single-doped $CoSb_{3-x}Te_x$.[19] In the

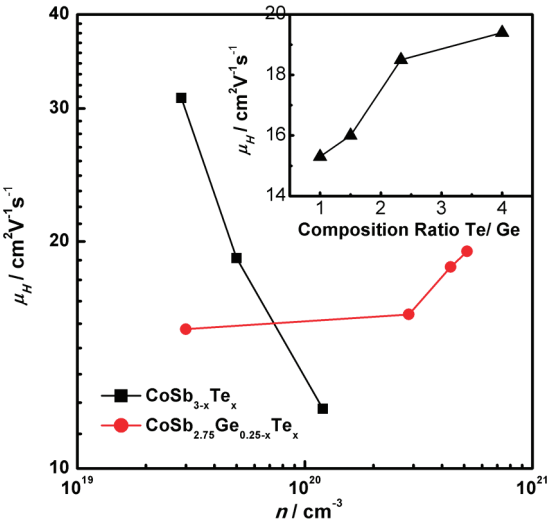

Figure 6. Room temperature Carrier mobility as a function of Carrier concentration for $CoSb_{2.75}Ge_{0.25-x}Te_x$. (Inset Figure: Room temperature Carrier mobility as a function of ratio of Te/Ge content for $CoSb_{2.75}Ge_{0.25-x}Te_x$).

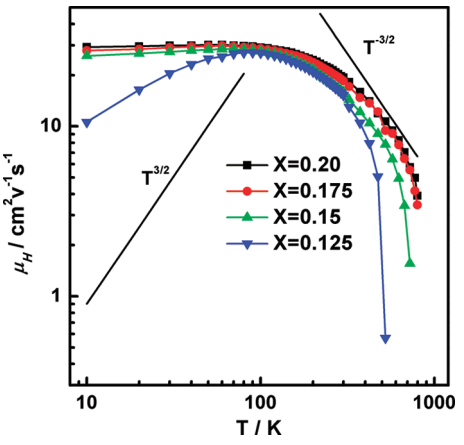

Figure 7. Carrier mobility as a function of temperature for $CoSb_{2.75}Ge_{0.25-x}Te_x$.

single-doped $CoSb_3$, the carrier mobility rapidly diminishes with the increasing content of Te, that is, with the increasing carrier density. In contrast, in the double-doped $CoSb_3$ (remember, the total amount of impurity is kept constant at 0.25) the mobility actually increases with the carrier density. This we interpret as a consequence of an apparently much stronger effect of Ge impurity on the mean-free path of electrons. As x increases, the Te content increases but at the expense of the Ge content, and with less Ge present the mobility seems to increase even though the Te impurity is more abundant. The inset shows this trend more clearly in the form of a plot of the composition ratio of Te to Ge versus the electron mobility.

The temperature dependence of the Hall mobility for $CoSb_{2.75}Ge_{0.25-x}Te_x$ (x = 0.125−0.20) compounds is shown in Figure 7. Uncompensated samples (x = 0.15, 0.175, and 0.20) display a very similar trend with the essentially T-independent mobility at low temperatures ($T \leq 100$ K) that then rapidly decreases at and above 300 K. In the temperature range 400−700 K, the mobility attains a $T^{-3/2}$ dependence characteristic of the

dx.doi.org/10.1021/cm200560s |Chem. Mater. 2011, 23, 2948–2955

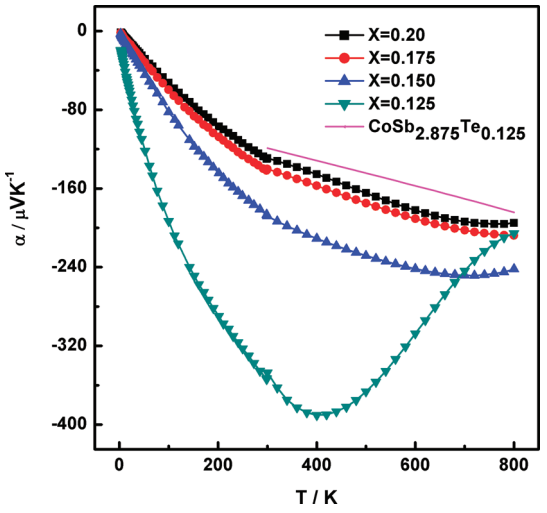

Figure 8. Seebeck coefficient as a function of temperature for $CoSb_{2.75}Ge_{0.25-x}Te_x$.

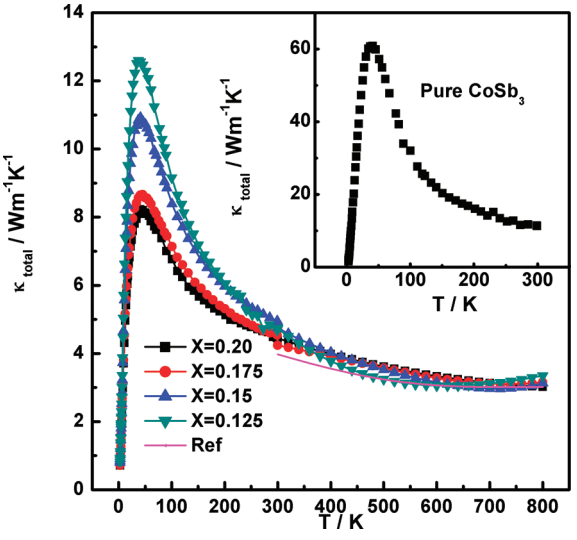

Figure 9. Thermal conductivity as a function of temperature for $CoSb_{2.75}Ge_{0.25-x}Te_x$. Solid line represents data of ref 19.

dominance of acoustic phonon scattering. At the highest temperatures the mobility decreases even faster, reflecting the contribution of optical phonons in scattering processes. We note a slight increase in the mobility with the increasing x, that is, the decreasing content of Ge, substantiating the data in the inset of Figure 6. The mobility of the compensated sample ($CoSb_{2.75}Ge_{0.125}Te_{0.125}$) with its highest Ge content tends distinctly toward the $T^{3/2}$ dependence below 100 K suggesting that impurity scattering is an important limiting mechanism in this sample.

The temperature dependence of the Seebeck coefficient α of $CoSb_{2.75}Ge_{0.25-x}Te_x$ (x = 0.125−0.20) compounds is shown in Figure 8. In the entire temperature range, the Seebeck coefficient of all specimens is negative in accord with the behavior of the Hall effect. For all noncompensated compounds, the absolute value of α increases with the increasing temperature at least up to 700 K. At the highest temperatures, the onset of intrinsic conduction is responsible for a turn around, and the magnitude of the Seebeck

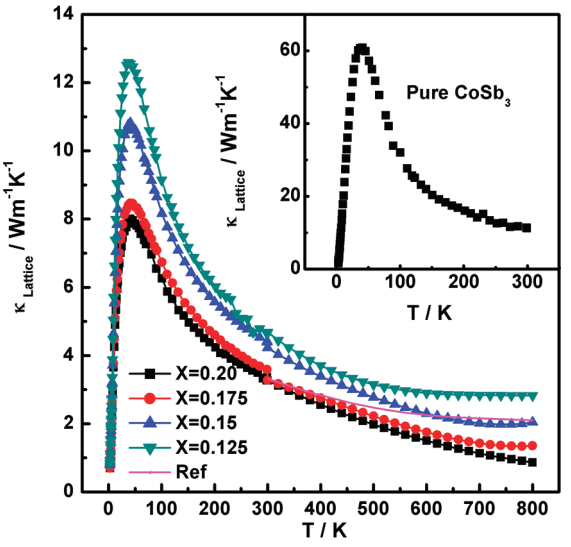

Figure 10. Lattice thermal conductivity as a function of temperature for $CoSb_{2.75}Ge_{0.25-x}Te_x$. Solid line represents data of ref 19.

coefficient starts to decrease. The magnitude of the Seebeck coefficient increases the closer the contents of Ge and Te are to each other. The exactly compensated sample (x = 0.125) has a much higher magnitude of the Seebeck coefficient, becomes intrinsic already above 400 K, and its magnitude falls rapidly at higher temperatures. Combining the electrical conductivity with the Seebeck coefficient, the power factor $\sigma\alpha^2$ reaches the maximum value of 4.40 × 10^{-3} W m^{-1} K^{-2} at 720 K for $CoSb_{2.75}Ge_{0.05}Te_{0.20}$.

Thermal Conductivity of $CoSb_{2.75}Ge_{0.25-x}Te_x$ (x = 0.125−0.20). Thermal conductivity as a function of temperature for different Te content is shown in Figure 9. In comparison with the undoped $CoSb_3$ (inset of Figure 9), the thermal conductivity of $CoSb_{2.75}Ge_{0.25-x}Te_x$ (x = 0.125−0.20) compounds is drastically reduced, especially at low temperatures. This is due to perturbations Te (and Ge) is making to the square planar ring structure of Sb. Since vibration frequencies of pnicogen rings fall within the range of frequencies of dominant modes of heat-carrying phonons,[16,17] Te (and Ge) substitutions on these rings are particularly effective in disrupting thermal transport. We also note that the peak in the thermal conductivity systematically decreases with the increasing Te content. Thus, while Ge appears more damaging to the transport of electrons, Te is more effective in limiting the mean-free path of phonons. Additional thermal conductivity reduction is due to the presence of nanostructural features (nanodots) shown in Figure 3 that are able to scatter long to midfrequency phonons.

The total thermal conductivity κ can be written as

$$\kappa = \kappa_L + \kappa_C \quad (1)$$

where κ_L and κ_C are the lattice and carrier thermal conductivity contributions, respectively. The carrier component (κ_C) can be calculated using the Wiedemann−Franz law as

$$\kappa_C = L\sigma T \quad (2)$$

where L is the Lorenz number, σ is the measured electrical conductivity, and T is the absolute temperature. In this study, we use the fully degenerate value of the Lorenz number L = 2.45 × 10^{-8} V^2/K^2. The lattice thermal conductivity is then obtained by

dx.doi.org/10.1021/cm200560s |Chem. Mater. 2011, 23, 2948–2955

subtracting κ_C from the total thermal conductivity, see Figure 10. With the increasing temperature, the lattice thermal conductivity decreases, and the trend regarding the dependence on the Te content extends to the highest temperatures. Thus, in comparison to the undoped $CoSb_3$ (see inset of Figure 10) the lattice thermal conductivity of $CoSb_{2.75}Ge_{0.25-x}Te_x$ ($x = 0.125-0.20$) compounds is reduced quite dramatically.

Substitution of Ge and Te on the ring-sites of Sb results in mass fluctuation scattering because of the mass difference of Te, Ge, and Sb atoms which, in turn, leads to a reduction in the lattice thermal conductivity. The scattering parameter A can be written in the form[21,26]

$$A = \frac{\Omega_0}{4\pi v^2} x(1-x)\left(\frac{\Delta M}{M}\right)^2 \quad (3)$$

Here, Ω_0, v, x, ΔM, and M stand for the volume of the unit cell, the sound velocity, the fraction of guest atoms, the atomic mass difference between the guest and host, and the average mass of the cell, respectively. According to this equation, the value of κ_L should increase with the increasing x because the atomic mass difference between Te and Sb, $\Delta M_{Te/Sb}$, is much smaller than that between Ge and Sb, $\Delta M_{Ge/Sb}$. The substitution of Ge atoms on Sb sites should thus decrease the thermal conductivity more dramatically than the substitution of Te atoms on Sb sites. In reality, an inverse effect is seen in our experiments. We argue that this is due to a larger number of Sb rings that must accommodate Te as x increases. Since Ge atoms preferentially occupy those Sb rings where Te is already present (a lower energy state because of charge compensation of Ge and Te), the number of distorted rings is determined by the number of available Te atoms. In our series of compounds, Ge atoms never exceed the number of Te atoms. Although the presence of Ge and Te-rich nanodots embedded in the skutterudite matrix is likely further reducing the thermal conductivity, the actual contribution is difficult to quantify in this limited series of samples against the background of strong point-defect scattering. The lowest lattice thermal conductivity is obtained for $CoSb_{2.75}Ge_{0.05}Te_{0.20}$ yielding the value of 0.87 W m^{-1} K^{-1} at 800 K. This value is comparable to the lattice thermal conductivity of filled skutterudites.[27−30]

Phonon Scattering Mechanism. Low values of the lattice thermal conductivity and the trend in the data indicate that perturbation of the ring structure of Sb is an important issue in heat transport of skutterudites. Consequently, we attempted to collect Raman spectra on our compounds by using a Renishaw Invia Raman system with a 514.5 nm excitation source and a spectra resolution of 1 cm^{-1}. The crystal symmetry *Im*3 implies eight Raman-active phonon modes related to vibrations of the pnicogen rings: 2 A_g + 2 E_g + 4 F_g where the A_g mode is single degenerate, the E_g mode is doubly degenerate, and the F_g mode is triply degenerate. The presence of Te and Ge on the rings of Sb is expected to alter the ring structure bonding, to lead to small changes in the d_1 and d_2 bond lengths, and to lower the symmetry of the ring.

Room temperature Stokes Raman spectra of $CoSb_3$ and $CoSb_{2.75}Ge_{0.05}Te_{0.20}$ are shown in Figure 11. Since no distinct peak was observed above 200 cm^{-1}, such data are omitted. Comparing Raman spectra for pure $CoSb_3$ with those of $CoSb_{2.75}Ge_{0.25-x}Te_x$ ($x = 0.125-0.20$) we note appreciable differences. The most notable one is the missing 134 cm^{-1} E_g peak (elongation of all sides of one rectangle, shortening of all sides of another)[16,17] in the spectrum of $CoSb_{2.75}Ge_{0.05}Te_{0.20}$. All other peaks seem to be slightly shifted to higher frequency when Ge and Te substitutes for Sb, see Table 2. This is due to a marginally smaller average mass of a ring that is occupied by Te and Ge in comparison to a ring occupied by Sb atoms only. The theoretical F_g4 mode (178 cm^{-1}) and A_g2 mode (179 cm^{-1}) are too close to each other, and we cannot distinguish them on either sample. The broadening of the two A_g modes in Te and Ge doped skutterudites in comparison to the pure $CoSb_3$ is due to disorder induced by the random distribution of the Te and Ge on the Sb rings.[31] The observed changes and shifts in the Raman spectrum indirectly confirm the accommodation of Te and Ge on the Sb rings.

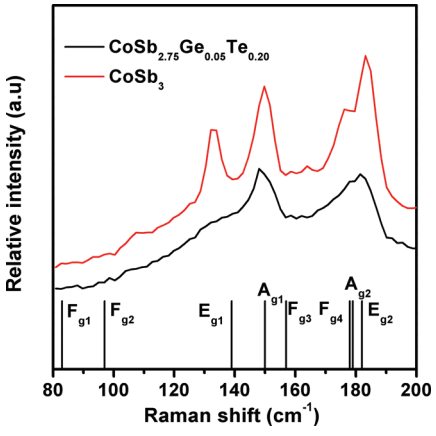

Figure 11. Raman shift of the samples $CoSb_3$ and $CoSb_{2.75}Ge_{0.05}Te_{0.20}$. The data of theoretical calculated modes for $CoSb_3$ from ref 23 are also presented.

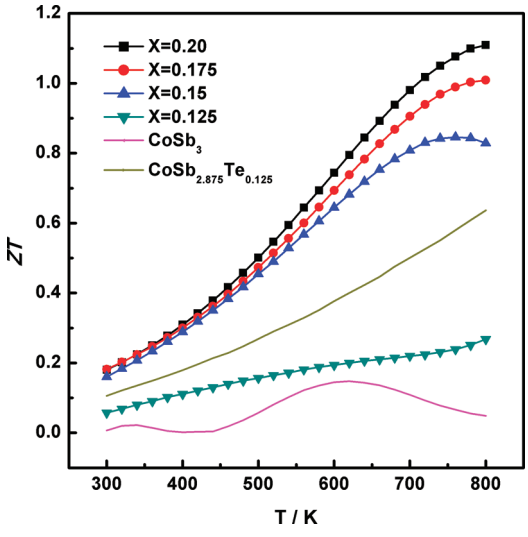

Figure 12. *ZT* as a function of temperature for $CoSb_{2.75}Ge_{0.25-x}Te_x$.

Table 2. Peak Position (cm^{-1}) of the Observed Raman-Active Phonon Modes in Skutterudites

$CoSb_3$ theory[17]	83(Fg1)	97Fg2	139(Eg)	150Ag	157Fg3	178Fg4	179(Ag)	182(Eg)
$CoSb_3$			133.94	148.034		176.156		181.419
$CoSb_{2.75}Ge_{0.05}Te_{0.20}$				149.794		177.911		183.173

dx.doi.org/10.1021/cm200560s |*Chem. Mater.* 2011, 23, 2948–2955

Dimensionless TE Figure of Merit *ZT*. The dimensionless TE figure of merit *ZT* for our compounds is calculated from the measured values of the electrical conductivity σ, the Seebeck coefficient α, and the thermal conductivity κ and is shown in Figure.12. *ZT* values of all samples increase with the increasing temperature and with the increasing content of Te. The highest ZT in the present series of samples is achieved with $CoSb_{2.75}Ge_{0.05}Te_{0.20}$ and reaches the value of 1.1 at 800 K. This represents nearly an order of magnitude increase over the figure of merit of pure $CoSb_3$[19] and the double-doped skutterudites are competitive with the best of single-filled n-type skutterudites.[27−30] The major beneficial factor is a much reduced lattice thermal conductivity that is dominated by point defect scattering which is augmented by the presence of in situ formed nanodots the origin of which is compositional variation between purely Sb occupied rings and rings accommodating Te and Ge impurities. The mechanism of the nanostructure formation seems akin to that of the LAST material where the regions of one composition are endotaxially embedded in a matrix of slightly different composition.[10,22,23]

CONCLUSIONS

Single-phase $CoSb_{2.75}Ge_{0.25-x}Te_x$ ($x = 0.125-0.20$) skutterudite compounds were synthesized using a melt-quench-anneal-SPS method. The samples possess nanostructural features consisting of circular domains of 30 nm diameter where the skutterudite phase is enriched with Ge and Te. These nanodots are uniformly dispersed in the skutterudite matrix that is poor in the content of Ge and Te. Energy considerations imply that Ge preferentially seeks pnicogen rings that already accommodate Te as the proximity of tetravalent Ge and hexavalent Te mimics the pentavalent site of Sb and neutralizes the change. The formation mechanism of this in situ nanostructure is similar to the case of nanostructures in the LAST materials.[10] The electrical transport properties can be modulated by adjusting the relative content of Ge and Te. Atoms of Ge and Te that substitute on the pnicogen rings alter the bonding and symmetry of the rings and cause appreciable changes in phonon vibration spectra. As a consequence, the thermal conductivity of these double-doped skutterudites is greatly suppressed in comparison to the thermal conductivity of a pure $CoSb_3$. Undoubtedly, point defect scattering is the dominant scattering mechanism of phonons and is made more effective by the presence of Ge that, moreover, enhances the solubility of Te in $CoSb_3$. Although we were unable to quantify the influence of the nanostructure on the thermal transport, the uniformly distributed nanodots with the caliper of 30 nm are of the right size to interact with long and midfrequency phonons and likely contribute to the overall low lattice thermal conductivity of these double-doped skutterudites. The TE figure of merit of our compounds is strongly enhanced in comparison to that of pure binary $CoSb_3$ and reaches values in excess of 1.1 at 800 K for $CoSb_{2.75}Ge_{0.05}Te_{0.20}$. Such high values of ZT are very competitive with the best values of single-filled skutterudites. It will be interesting to apply this double-doping approach in the fabrication of filled skutterudites with the hope of achieving n-type TE materials with very high *ZT*.

AUTHOR INFORMATION

Corresponding Author

*E-mail: tangxf@whut.edu.cn (X.T.), cuher@umich.edu (C.U.).

ACKNOWLEDGMENT

This work is sponsored by the National Basic Research Program of China (Grant 2007CB607501), National Science Foundation of China (Grants 50672118, 50731006, and 50820145203) and the 111 Project of China (Grant B07040). The work at the University of Michigan (low temperature transport studies and high temperature Hall effect measurements) is supported by the Center for Solar and Thermal Energy Conversion, an Energy Frontier Research Center funded by the U.S. Department of Energy, Office of Science, Office of Basic Energy sciences under Award Number DE-SC00000957. X.S. wishes to thank the China Scholarship Council (CSC) for support in the form of a partial fellowship (No. 2010695029).

REFERENCES

(1) Tritt, T M *Science* **1999**, *283*, 804.
(2) Slack, G A In *CRC Handbook of Thermoelectrics*; CRC: Boca Raton, FL, 1995.
(3) Rowe, D. M. *Thermoelectrics Handbook: Macro to Nano*; CRC/Taylor & Francis: Boca Raton, FL, 2006.
(4) Uher, C. *Recent Trends in Thermoelectric Materials Research I, Semiconductors and Semimetals*; Academic Press: San Diego, CA, 2001.
(5) Caillat, T.; Borshchevsky, A.; Fleurial, J. P. *J. Appl. Phys.* **1996**, *80*, 4442.
(6) Morelli, D. T.; Meisner, G. P. *J. Appl. Phys.* **1995**, *77*, 3777.
(7) Morelli, D. T.; Meisner, G. P.; Chen, B. X.; Hu, S. Q.; Uher, C. *Phys. Rev. B* **1997**, *56*, 7376.
(8) Shi, X.; Kong, H.; Li, C. P.; Uher, C.; Yang, J.; Salvador, J. R.; Wang, H.; Chen, L.; Zhang, W. *Appl. Phys. Lett.* **2008**, *92*, 182101.
(9) Hicks, L. D.; Dresselhaus, M. S. *Phys. Rev. B* **1993**, *47*, 12727.
(10) Hsu, K. F.; Loo, S.; Guo, F.; Chen, W.; Dyck, J. S.; Uher, C.; Hogan, T.; Polychroniadis, E. K.; Kanatzidis, M. G. *Science* **2004**, *303*, 818.
(11) Xie, W. J.; He, J.; Kang, H. J.; Tang, X. F.; Zhu, S.; Laver, M.; Wang, S. Y.; Copley, J. R. D.; Brown, C. M.; Zhang, Q. J.; Tritt, T. M. *Nano Lett.* **2010**, *10*, 3283.
(12) Li, H.; Tang, X. F.; Zhang, Q. J.; Uher, C. *Appl. Phys. Lett.* **2009**, *94*, 102114.
(13) Sootsman, J. R.; Pcionek, R. J.; Kong, H.; Uher, C.; Kanatzidis, M. G. *Chem. Mater.* **2006**, *18*, 4993.
(14) Androulakis, J.; Lin, C. H.; Kong, H. J.; Uher, C.; Wu, C. I.; Hogan, T.; Cook, B A.; Caillat, T.; Paraskevopoulos, K. M.; Kanatzidis, M. G. *J. Am. Chem. Soc.* **2007**, *129*, 9780.
(15) Xiong, Z.; Huang, X. Y.; Chen, X. H.; Ding, J.; Chen, L. D. *Scr. Mater.* **2010**, *62*, 93.
(16) Dimitrov, I. K.; Manley, M. E.; Shapiro, S. M.; Yang, J.; Zhang, W.; Chen, L. D.; Jie, Q.; Ehlers, G.; Podlesnyak, A.; Camacho, J.; Li, Q. *Phys. Rev. B* **2010**, *82*, 174301.
(17) Feldman, J. L.; Singh, D. J. *Phys. Rev. B* **1996**, *53*, 6273.
(18) Liu, W. S.; Zhang, B. P.; Li, J. F.; Zhang, H. L.; Zhao, L. D. *J. Appl. Phys.* **2007**, *102*, 103717.
(19) Li, X. Y.; Chen, L. D.; Fan, J. F.; Zhang, W. B.; Kawahara, T.; Hirai, T. *J. Appl. Phys.* **2005**, *98*, 083702.
(20) Liu, W. S.; Zhang, B. P.; Zhao, L. D.; Li, J. F. *Chem. Mater.* **2008**, *20*, 7526.
(21) Yang, J. H.; Meisner, G. P.; Morelli, D. T.; Uher, C. *Phys. Rev. B* **2000**, *63*, 014410.
(22) Quarez, E.; Hsu, K. F.; Pcionek, R.; Frangis, N.; Polychroniadis, E. K.; Kanatzidis, M. G. *J. Am. Chem. Soc.* **2005**, *127*, 9177.
(23) Biswas, K.; He, J. Q.; Zhang, Q. CH.; Wang, G. Y.; Uher, C.; Dravid, V. P.; Kanatzidis, M. G. *Nat. Chem.* **2011**, *3*, 160.
(24) Mandrus, D.; Migliori, A.; Darling, T. W.; Hundley, M. F.; Peterson, E. J.; Thompson, J. D. *Phys. Rev. B* **1995**, *52*, 4926.
(25) Dyck, J. S.; Chen, W.; Yang, J. H.; Meisner, G. P.; Uher, C. *Phys. Rev. B* **2002**, *65*, 115204.

(26) Meisner, G. P.; Morelli, D. T.; Hu, S.; Yang, J. H.; Uher, C. *Phys. Rev. Lett.* **1998**, *80*, 3551.
(27) Puyet, M.; Lenoir, B.; Dauscher, A.; Dehmas, M.; Stiewe, C.; Muller, E. *J. Appl. Phys.* **2004**, *95*, 4852.
(28) Nolas, G. S.; Kaeser, M.; Littleton, R. T., IV; Tritt, T. M. *Appl. Phys. Lett.* **2000**, *77*, 1855.
(29) Li, H.; Tang, X. F.; Su, X. L.; Zhang, Q. J. *Appl. Phys. Lett.* **2008**, *92*, 202114.
(30) Li, H.; Tang, X. F.; Su, X. L.; Zhang, Q. J.; Uher, C. *J. Phys. D: Appl. Phys.* **2009**, *42*, 14540.
(31) Nolas, G. S; Kendziora, C. A. *Phys. Rev. B* **1999**, *59*, 6189.